Analysis of L and C-bands SAR images time series over a Sahelian area

Pierre Louis Frison, Grégoire Mercier, G. Faye, Éric Mougin, Pierre Louis Hiernaux, Cédric Lardeux, J.P. Rudant

Analysis of L- and C-Band SAR Image Time Series Over a Sahelian Area

P.-L. Frison, G. Mercier, G. Faye, E. Mougin, P. Hiernaux, C. Lardeux, and J.-P. Rudant

***Abstract*—This letter presents an analysis of two synthetic aperture radar (SAR) images time series over a Sahelian area, which is located in the Gourma region, Mali. The first one is acquired at the C-band by the Environment Satellite–Advanced SAR sensor in wide swath (WS) mode and the second one at the L-band by the ALOS–Phased Array-type L-band SAR in fine, dual, and WS modes. A change detection method based on random projection and the hue–saturation–value transform appears to be very well appropriated to detect the temporal changes appearing on both data sets. The results illustrate the higher penetration depth of the L-band over such sandy soils. The C-band time series is found to be very sensitive to surface changes (soil moisture and vegetation growth). By contrast, the L-band time series appear to be very stable over the sandy soils, i.e., the only temporal changes occurring over temporary or permanent ponds.**

***Index Terms*—ALOS/Phased Array-type L-band SAR (PALSAR), ENVISAT/Advanced Synthetic Aperture Radar (ASAR), Mali, radar, Sahel, semiarid regions, synthetic aperture radar (SAR), time series analysis.**

I. Introduction

SINCE the launch of the European Remote Sensing 1 (ERS-1) synthetic aperture radar (SAR) in 1991, land surfaces have been continuously observed by numerous spaceborne SAR sensors in different configurations and frequencies, i.e., at X-, C-, and L-bands. C-band radar data have shown their potential for the monitoring of semiarid areas, allowing the estimation of vegetation biomass and/or soil moisture content. Past studies have shown that over semiarid Sahelian areas characterized by rather low vegetation cover ($< 30\%$) and biomass (< 1.5 ton dry matter per hectare), C-band radar data are both sensitive to vegetation and soil parameters (roughness and soil moisture), [1], [2]. On the other hand, the L-band larger wavelength should significantly reduce the vegetation contribution in the radar signal that should be largely dominated by the soil contribution. In order to make a deeper comparison between the differences observed at the C- and L-bands over Sahelian areas, two time series acquired by ENVISAT–Advanced SAR (ASAR) and ALOS–Phased Array-type L-band SAR (PALSAR) sensors over the Gourma region, Mali, are analyzed. A particular attention is put on the temporal changes that are observed over the two time series, allowing the analysis of the sensitivity of both frequencies to the seasonal variation of surface features.

The first section presents the study site and the data used in the study. The change detection method is detailed in the second section. The results are then discussed.

P.-L. Frison, G. Faye, C. Lardeux, and J.-P. Rudant are with the Université Paris-Est, ESYCOM laboratory (EA 2552), UPEMLV, ESIEE-Paris, CNAM, F-77454 Marne-la-Vallée, France (e-mail: frison@univ-mlv.fr).

G. Mercier is with Télécom Bretagne, Sciences et Techniques de l'Information, de la Communication, et de la Connaissance/Connaissance, Information, Décision Laboratory, Unité Mixte de Recherche 6285, Technopole Brest-Iroise, 29238 Brest, France (e-mail: gregoire.mercier@telecom-bretagne.eu).

E. Mougin and P. Hiernaux are with the Geosciences Environnement Toulouse Laboratory, UMR Centre National de la Recherche Scientifique 5563, 31400 Toulouse, France (e-mail: eric.mougin@get.ops-mip.fr).

II. Study Site and Data

A. Study Site

The study site (1° W–2° W, 14.5° N–17.5° N) is located within the Sahelian zone, in the Gourma region, which stretches from the loop of the Niger River southward down to the state border with Burkina-Faso [3].The region experiences a single rainy season with most precipitation falling between late June and mid-September with mean annual rainfall ranging from about 150 to 600 mm along this north–south transect. The rainy season is followed by a long dry season of eight months in the south increasing to ten months in the north. The vegetation consists in a herbaceous layer almost exclusively composed of annual plants and a sparse woody plant population (mean cover below 5%).The phenology of vegetation is mainly determined by rainfall. Grass development starts after the first rains in June or July, and senescence approximately coincides with the end of the rainy season. There is no green vegetation during the dry season, a part from a few shrubs foliage.

The underlying geology of the Gourma region includes precambrian sandstone and schist eroded into a peneplain surface with occasional plateaus of hard sandstones that have resisted erosion. The Gourma peneplain is at between 250- and 330-m altitude with the highest isolated sandstone buttes reaching 900–1100 m. The eroded and exposed peneplain surfaces are locally capped by an iron pan formed during the humid period of the Tertiary, but larger areas of the region are covered by deep and stabilized sand dunes deposited during arid periods of the Quaternary. In addition to these two major landforms and also inherited from the humid periods of the Quaternary, remnants of alluvial systems and lacustrine depressions can be observed. At mesoscale, soil types can be gathered into three main categories: sandy soils extending over 58% of the area, shallow soils on rock and hard pan outcrops extending on 23.3%, and fine textured soils in low lands on 18.7%. The land units are presented in Fig. 1(a). They correspond to the dominant category ($> 66\%$) and are labeled "mosaic" otherwise.

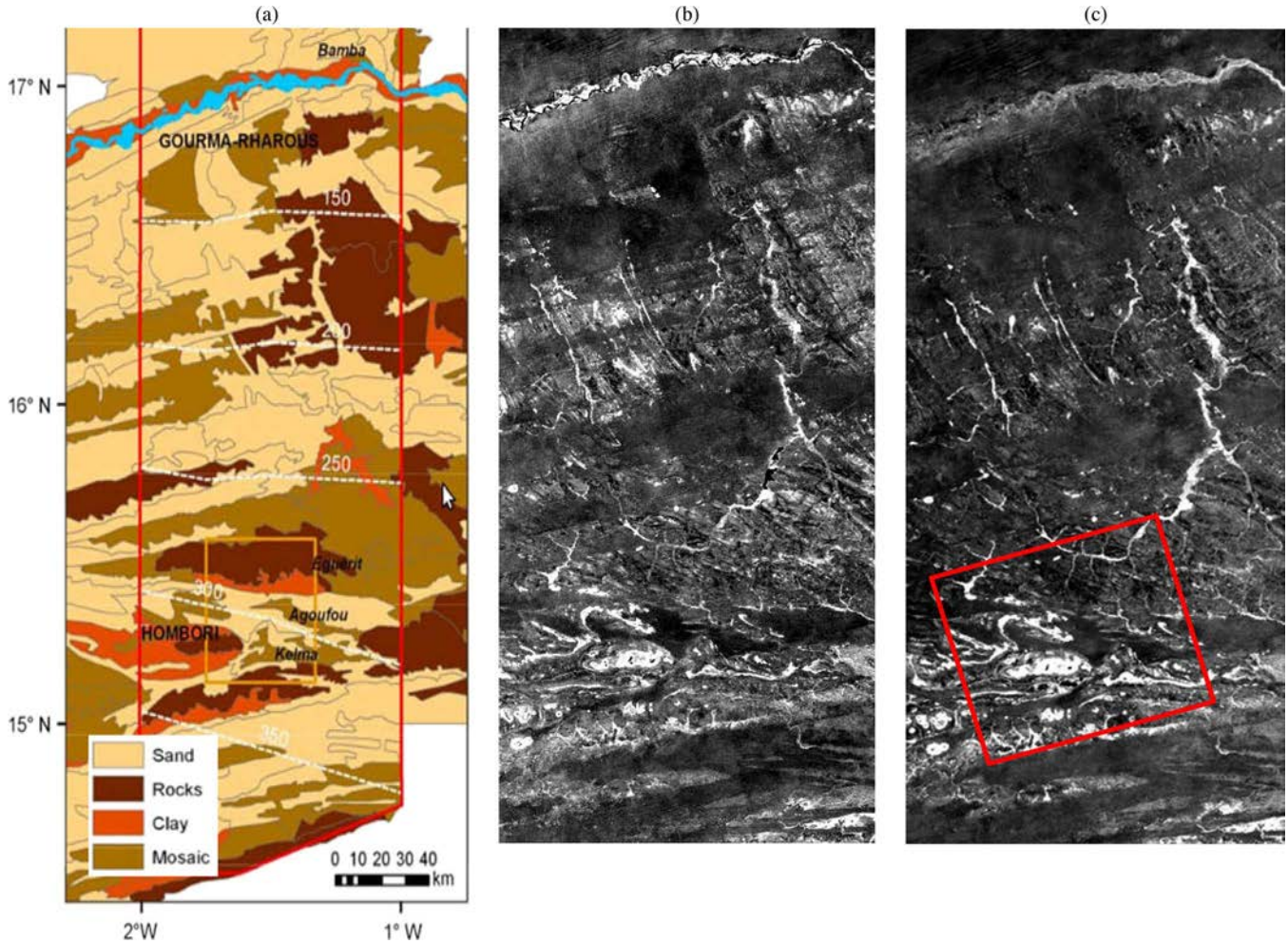

Fig. 1. (a) Soil-type map of the study site in Gourma, Mali. (b) Radar image acquired in WS mode at the C-band by ASAR on December 16, 2005. (c) Radar image acquired at the L-band by PALSAR on January 1, 2008.The red square corresponds to the acquisition area of PALSAR images in fine beam mode.

B. SAR Data

Two data sets are analyzed; they have been acquired at the C- ($\lambda = 5.6$ cm) and L-bands ($\lambda = 23.6$ cm) by the ASAR and PALSAR sensors, respectively. Five ASAR acquisitions have been realized between September 29 and December 16, 2005, at 35-day intervals. They have been acquired at HH polarization in wide swath (WS) mode with 150 m of spatial resolution. For these acquisitions, the study site is located at an incidence angle of about 40°. 17 PALSAR acquisitions have been made between July 2007 and May 2009: 12 in Fine beam mode (seven in Single HH and five in Dual HH/HV polarization) with 15 m of spatial resolution, and five in Wide beam mode (i.e. 100 m of spatial resolution) at HH polarization. The study site corresponds to incidence angles of about 40° and 35° for fine beam and WS modes, respectively.

III. Change Detection Method

Change detection in remote sensing image series may be difficult due to artifacts, such as scalloping, that where present on some of the studied images. Moreover, the high dynamic range of the gray tone values and the presence of speckle (even after filtering process) in radar images make inefficient traditional methods based on the analysis of the relative differences or ratio. The extension proposed in [4] that is based on a Kullback–Leibler divergence of the local statistics cannot be used here because the change detection process is applied on a time series and not on the comparison between two dates.

The change detection technique has to balance between the detection of highest variability between seasonal land cover and the mitigation of false detection due to the differences in the observation conditions. In order to reduce artifacts due to speckle, a multilooking process is made by applying a boxcar filter uniformly to the images. The size of the local window is 10×10 on fine beam mode images and 4×4 pixels on WS mode images.

One of the usual change detection methods from a long time series is based on the principal component (PC) analysis because it is often considered that the axis hooded by the second highest eigenvalue is related to changes [5], under the hypothesis that the change areas are much less representative (statistically) than the no change areas. In such a representation, the pixels of image time series are considered to be vector-pixels in a feature space whose dimension is equal to the number of acquisitions. When no change occurs, the vector pixels have components that are distributed along the mean axis (hooded by the eigenvector associated to the highest eigenvalue), which corresponds to a normal evolution in the time series. On the contrary, when a change occurs at a specific date and a specific location, the components of the related pixel are becoming

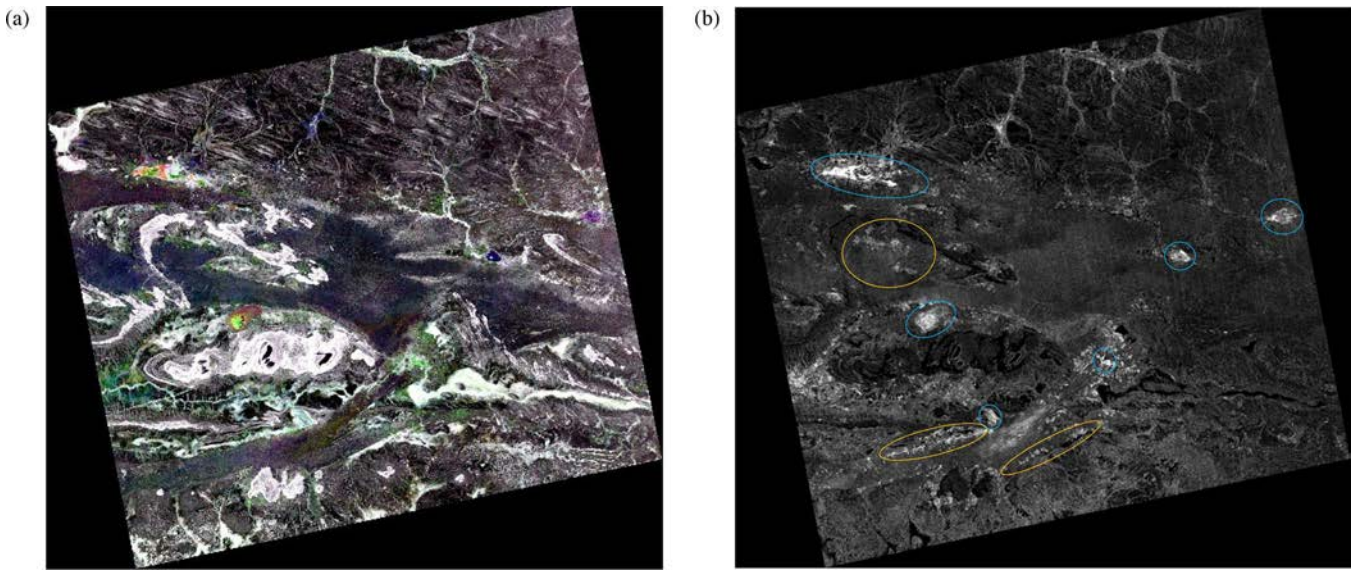

Fig. 2. (a) Temporal color composite image of PALSAR fine beam acquisitions (HH polarization) (R: January 17, 2007, G: October 20, 2007, B: January 22, 2009). (b) Change detection images obtained for the 12 fine beam PALSAR images time series (HH polarization). Water ponds and millet fields are surrounded in blue and orange, respectively.

different from the "normal" components so that the vector pixel is moving away from the mean axis. Unfortunately, the use of the second eigenvector for characterizing changes is not relevant for the considered SAR image series. In fact, the variability induced by the scene and the SAR sensor make changes through isotropic directions away from the mean axis, so that the second PC holds only partial information of the changes. As a consequence, the distance to the mean axis appears to be a valuable alternative. Hence, if we consider change detection from a set of three images, the second and third PCs should be required to define the distance of the mean axis. In a 3-D space, this distance to the main axis appears to be similar to the saturation measure from the hue–saturation–value (HSV) color transform. In this case, the involved distance is similar (but not equivalent) to the Euclidean distance, and for which details may be found in [6]. However, in N-D feature space ($N > 3$), it is difficult to choose the good PC axes or the appropriated subspace to highlight changes. Then, this approach should be implemented in a reduced dimension feature space to cope with reasonable memory requirement and computation space. In [7], it has been stressed that an appropriated time series image classification could be restricted to a very limited number of images if those images correspond to the key period of temporal change. In the present application, no *a priori* criterion has been found to select the most appropriated images. Thus, a random projection technique has been applied. This strategy remains valuable only if the number of images in the time series is important, if not, a simple exhaustive search has to be used.

From the N images in the time series, three acquisitions are chosen randomly. They are considered as components of a red–green–blue (RGB) false color representation. This color space is transformed in the HSV representation [6]. Then, the saturation channel is considered to be representative of changes in-between the three selected images. The process is iterated K times, and the mean of the saturation channels serves the change measure of the time series. For $N \leq 6$, the combination may be performed through an exhaustive selection of triplets yielding C_3^N combinations ($C_3^N \leq 20$). When $N > 6$, the three channels are randomly chosen and the process is repeated K times (with K arbitrary chosen to 50 in the present case). It is worth noting that the radiometric-based change detection procedure is sensitive to the differences in radiometry so that a special care has to be brought to the image intercalibration.

IV. Results and Discussion

Fig. 1(b) and (c) shows the study site acquired by the ASAR and PALSAR sensors on December 16, 2005 and January 1, 2008, respectively, both in WS mode. On the whole, the two images are similar. The Niger River is the bright line crossing the top of the image. The sandy soils correspond to darker zones. The bright patterns correspond either to relief (buttes and rock or hard pan outcrops, as for the center of the red square) or to lowlands [as for the bottom right of the red square in Fig. 1(c)], which are characterized by very rough and surfaces concentrating the trees that can be encountered over the study site. Bright linear structures correspond also to the remnants of alluvial systems, which are clearly visible on both images. However, they are better discriminated at the L-band due to the higher penetration depth in sandy soils for lower frequencies. In particular, the sand dunes, up to 10 m thick, oriented from west to east, appear with the C-band [see Fig. 1(b)] in alternate dark and lighter rectilinear structures in the upper third of the image, whereas they are not visible with the L-band [see Fig. 1(c)].

The sensitivity of L- and C-bands to seasonal changes have been analyzed by applying the change detection algorithm presented in Section III to different time series. First, a special analysis has been made on the PALSAR data acquired at fine beam mode at HH polarization, as these 12 acquisitions form the most consistent time series of the whole PALSAR data set. Temporal color composite image acquisitions made at three different dates at HH polarization is given in Fig. 2(a). The corresponding acquisition area is the red square shown in Fig. 1(c). The change detection result is presented in Fig. 2(b). The efficiency of the algorithm is worth noticing, enabling to account for the stable temporal behavior of the main relief

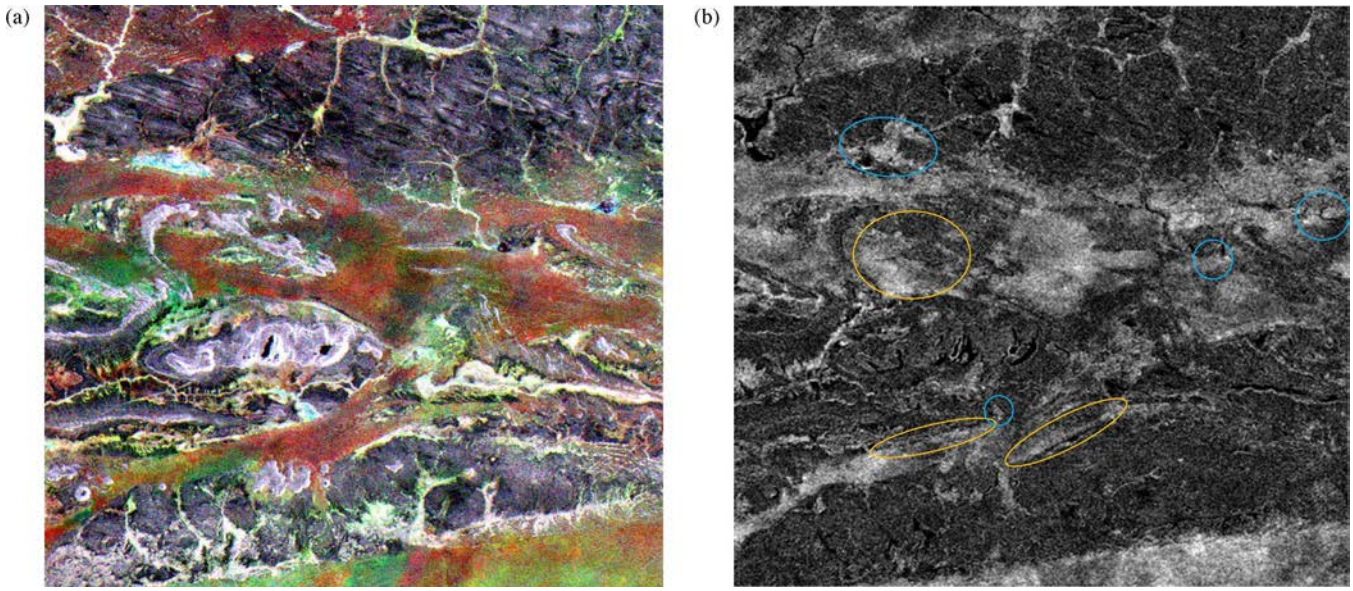

Fig. 3. (a) Temporal color composite image of ASAR WS acquisitions (HH polarization) (R: July 29, G: October 7, B: November 11, 2005). (b) Change detection images obtained for the five ASAR image time series (HH polarization). Water ponds and millet fields are surrounded in blue and orange, respectively.

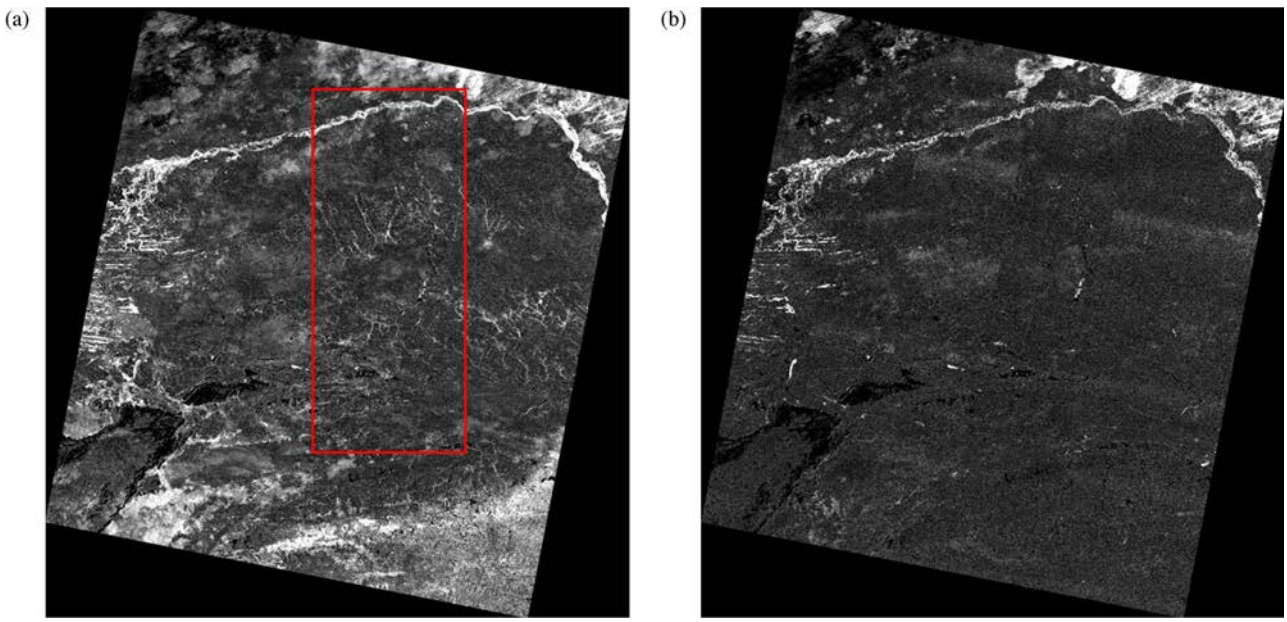

Fig. 4. a) Change detection obtained for the five PALSAR wide beam acquisitions (HH polarization). (b) Change detection images obtained for the three PALSAR wide beam images acquired during the dry season (HH polarization).

structures or lowlands, which appear in black, independently of the high values observed on the intensity images. The rock and hard pan outcrops on the upper right corner also show a stable behavior, whereas the brighter color of the remnant alluvial system indicates that it is still temporary active with rainwater runoff. The brightest features correspond to millet fields (surrounded in orange) and to water ponds (surrounded in blue), indicating the high temporal change observed with respect to their extent and surface state (roughness and aquatic vegetation). Finally, the sandy soils (central part of the scene for example) exhibit low temporal changes, indicating the low sensitivity of the L-band to surface roughness and moisture as well to the herbaceous layer development over such semiarid areas.

For comparison with the C-band, a temporal color composite image is presented over the same subscene extracted from the ASAR WS acquisitions [see Fig. 3(a)]. The result of the temporal change algorithm obtained from the five WS acquisitions is shown in Fig. 3(b). Similarly to the L-band, the main relief, lowlands, and rock or hard pan outcrops appear in dark tones in Fig. 3(b), traducing a stable temporal behavior. The most striking difference with the L-band concerns the sandy soils, which appear as bright as water ponds and millet fields. It illustrates the high sensitivity of the C-band to surface state (surface roughness, soil moisture, and vegetation development) over such semiarid regions [8]. The wide extent of these areas induce confusion with millet fields and water ponds, which exhibit also

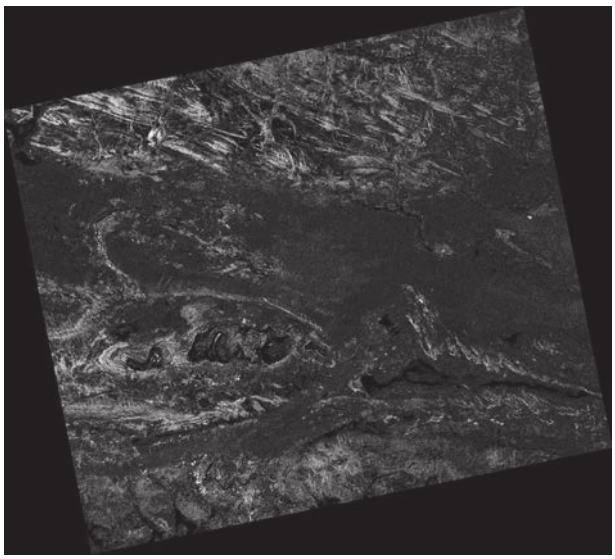

Fig. 5. Change detection observed between HH and HV polarizations for the five PALSAR dual-mode acquisitions.

significant temporal changes, leading the interpretation of this image less obvious than for the L-band.

As an illustration, Fig. 4 shows the temporal change detection obtained over a wider region with PALSAR acquisitions in wide beam mode (red rectangle corresponds to the area in Fig. 1). Fig. 4(a) shows the change detection applied to the five wide beam acquisitions, whereas Fig. 4(b) shows the change for the three acquisitions realized during the dry season. The main water ponds are easily discriminated on both images, i.e., the permanent ponds corresponding to those detected during the dry season [see Fig. 4(b)] and the temporary ponds corresponding to those detected during both dry and wet season [see Fig. 4(a)]. Water ponds detection is of prime interest: First, they consist in the main water resource in the Sahel for both livestock and people. In addition, they are a marker of hydrological processes change [9].

To analyze the influence of polarization, the same change detection method has been applied to the five dual HH/HV PALSAR acquisitions. In that case, HH acquisition has been affected to both R and G channels, and the HV acquisition has been affected to the B channel, before performing the RGB-to-HSV transform. Fig. 5 presents the mean changes observed between HH and HV polarizations, i.e., corresponding to average of the five saturation obtained. Sandy soils appear in dark tones, traducing the small differences observed between HH and HV polarizations at the L-band over such surfaces. By contrast, bright patterns correspond to either water ponds or rock and hard pan outcrops (top of the image), resulting to a larger difference between HH and HV over these surfaces than for sandy or shallow soils. These signatures occur over areas characterized by predominant surface scattering mechanisms. On the other hand, structures with a high radar response (i.e., appearing in white in the RGB space in Fig. 2(a)], such as main relief features, lowlands, or the remnant alluvial system, appear in dark tones in Fig. 5. Indeed, such white colored features in both polarizations are associated to very low saturation values.

V. Conclusion

A change detection method based on random projection and the HSV representation appears well adapted to highlight changes over different SAR image sets. This algorithm, which is easy to use and of limited complexity, allowed the analysis of temporal change detection between L- and C-band SAR time series over a Sahel region. The results show that temporal changes at the L-band are observed over water ponds and millet fields, whereas sandy soils observe a rather temporal stable behavior. They indicate the low sensitivity of the L-band to roughness state and moisture of the surface as well to the herbaceous layer development over such semiarid areas. The comparison of radar intensity images between L- and C-bands illustrates the higher penetration depth of the L-band for the sandy soils, allowing a better discrimination of remnant alluvial systems than at the C-band. With respect to the C-band, in addition to water ponds and millet fields, sandy soils show also significant temporal changes due to the high sensitivity of the C-band to both vegetation and soil moisture and roughness over such areas. This analysis shows that L-band radar data is well suited for the detection of temporal or permanent ponds in the Sahelian region.

Acknowledgment

The authors thank ESA for providing ASAR and PALSAR data (CAT-1 Project ID 4229).

References

[1] L. Jarlan, E. Mougin, P. Frison, L. Mazzega, and P. Hiernaux, "Analysis of ERS wind scatterometer time series over Sahel (Mali)," *Remote Sens. Environ.*, vol. 81, no. 2/3, pp. 404–415, Aug. 2002.

[2] F. T. Ulaby, R. K. Moore, and A. K. Fung, *Microwave Remote Sensing Active and Passive—Vol. III: From Theory to Applications*. Norwood, MA: Artech House, 1986.

[3] E. Mougin, P. Hiernaux, L. Kergoat, M. Grippa, P. de Rosnay, F. Timouk, V. Le Dantec, V. Demarez, F. Lavenu, M. Arjounin, T. Lebel, N. Soumaguel, E. Ceschia, B. Mougenot, F. Baup, F. Frappart, P. L. Frison, J. Gardelle, C. Gruhier, L. Jarlan, S. Mangiarotti, B. Sanou, Y. Tracol, F. Guichard, V. Trichon, L. Diarra, A. Soumaré, M. Koi, F. Dembélé, C. Lloyd, N.P. Hanan, C. Damesin, C. Delon, D. Serca, C. Galy-Lacaux, J. Seghieri, S. Becerra, H. Dia, F. Gangneron, and P. Mazzega, "The AMMA Gourma observatory site in Mali: Relating climatic variations to changes in vegetation, surface hydrology, fluxes and natural resources," *J. Hydrol.*, vol. 375, no. 1/2, pp. 14–33, 2009.

[4] J. Inglada and G. Mercier, "A new statistical similarity measure for change detection in multitemporal SAR images and its extension to multiscale change analysis," *IEEE Trans. Geosci. Remote Sens.*, vol. 45, no. 5, pp. 1432–1446, May 2007.

[5] T. Celik, "Unsupervised change detection in satellite images using principal component analysis and k-means clustering," *IEEE Geosci. Remote Sens. Lett.*, vol. 6, no. 4, pp. 772–776, Oct. 2009.

[6] A. Kruse and L. Raines, "A technique for enhancing digital color images by contrast stretching in Munsell color space," in *Proc. ERIM 3rd Thematic Conf.*, Ann Arbor, MI, 1984, pp. 755–760.

[7] J. Inglada and S. Garrigues, "Land-cover maps from partially cloudy multi-temporal image series: Optimal temporal sampling and cloud removal," in *Proc. IEEE IGARSS*, 2010, pp. 3070–3073.

[8] L. Jarlan, E. Mougin, P.-L. Frison, P. Mazzega, and P. Hiernaux, "Analysis of ERS wind scatterometer time series over Sahel (Mali)," *Remote Sens. Environ.*, vol. 81, no. 2, pp. 404–413, Aug. 2002.

[9] J. Gardelle, P. Hiernaux, L. Kergoat, and M. Grippa, "Less rain, more water in ponds: A remote sensing study of the dynamics of surface waters from 1950 to present in pastoral Sahel (Gourma region, Mali)," *Hydrol. Earth Syst. Sci.*, vol. 14, no. 2, pp. 309–324, 2010.